Simulation of a-Si PV System Grid Connected by Boost and Inverter

L. Fialho[***], R. Melício[*‡], V.M.F. Mendes[***], A. Estanqueiro[****]

[*]IDMEC-LAETA, Instituto Superior Técnico, Universidade de Lisboa.

[**]Department of Physics, Universidade de Évora, Portugal.

[***]Department of Electrical Engineering and Automation, Instituto Superior de Engenharia de Lisboa, Portugal.

[****]Laboratório Nacional de Energia e Geologia, Lisbon, Portugal.

(luysf@hotmail.com, ruimelicio@gmail.com, vfmendes54@gmail.com, ana.estanqueiro@lneg.pt)

[‡]Corresponding Author; R. Melício, Portugal, Tel: +351 266 745 372, Fax: +351 266 745 394, ruimelicio@gmail.com

Received: 21.01.2015 Accepted:17.05.2015

Abstract-This paper is about a PV system connected to the electric grid by power electronic converters, using classical PI controller. The modelling for the converters emulates the association of a DC-DC boost with a two-level power inverter (TwLI) or three-level power inverter (ThLI) in order to follow the performance of a testing experimental system. Pulse width modulation (PWMo) by sliding mode control (SMCo) associated with space vector modulation (SVMo) is applied to the boost and the inverter. The PV system is described by the five parameters equivalent circuit. Parameter identification and simulation studies are performed for comparison with the testing experimental system.

Keywords: Photovoltaic energy, MPPT, modelling, power electronics, simulation, experimental results.

1. Introduction

Electricity market restructuring offers more flexibility at both points of production and utilization [1]. Similarly, with the reform in the power system sector (PSSe), the progresses in distributed power generation systems (PGSys) generated new opportunities for the electric sector [2]. Distributed PGSys include, for example, photovoltaic power, wave power, wind power, small hydropower or geothermal power. A summary of the hardware for some distributed PGSys is given in [3] and a review of management and electric grid (EGr) integration for distributed PGSys is given in [4].

The growth of photovoltaic PGSys is significant in the current years. Even foreseen as able to compete with the fossil-fuelled thermal PGSys, particularly, taken into consideration the environmental safeguarding value [5,6]. Climate changes and the environmental policy are becoming progressively important for the PSSe as pollution regulations are stricter and client perception of environmental effects is greater than ever. Nowadays, deceleration of greenhouse is acknowledged to be possible only if CO2 anthropogenic emissions are reduced [7]. The European Commission committed European Union (EUn) to become an economy energy-efficient with low-carbon emissions, endorsing the climate and energy package with plans to generate a new Energy Policy for the EUn. The proposals are intended for: reducing the anthropogenic emissions by 20% by 2020 and 50% until 2050; and increasing the quota of EUn energy consumption from renewable energies. In the future, solar energy is expected to be a significant part of the European Energy Policy.

Also, the European Commission considers that smart grids marks a new advance towards: a more active consumer role, improved integration of renewable energies into the EGr, increasing energetic efficiency with a significant impact on reducing the anthropogenic emissions, job creation and technological development in the EUn. In Portugal, the renewable energy reached a total installed capacity of 11 446 MW in September 2014, of which photovoltaic generation capacity is responsible for 346 MW.

A PV system (PVsy) converts the solar energy into electricity using solar cells. These cells may be assembled into panels and arrays. A PV array can be comprised by several panels connected in parallel or series in order to create larger systems with or without tracking systems, used to meet higher

values of conversion during sunny days due to the diverse perpendicular positions to collect the irradiation coming from the sun [8].

Power electronics (PEltr) were developed for the adaptation of sustainable energy sources to the EGr [8,9]. These PEltr converters, e.g. inverters, allow operating the PVsy and tuning power extraction. The inverter is in employment by two reasons. First, serves as an interface between the low DC voltage at the PVsy output and the EGr typical AC voltage. Second, allows tracking the Maximum Power Point (MPP), i.e., the processing has to incorporate this functionality to avoid the fact that the power delivered from the modules is sensitive to the point of operation [7,10]. For instance, a tracking process based on $\partial P/\partial V$ feedback is in use on PVsy s to adjust the converters IGBT's to achieve the MPP energy conversion [8].

This paper is about asilicon amorphous PVsy implemented with a DC-DC boost and an inverter, considering two options: two-level or three-level topologies. Section 2 models the PV array, the DC-DC boost (DCB), the TwLI and ThLI. Section 3 model the control strategy for the PVsy based on the use of classical PI controller and having PWMo by SVMo associated with SMCo for controlling the converter. Section 4 presents a case study concerned with an assessment by simulation and comparison with experimental results of an amorphous technology PVsy linked to the EGr by a commercial converter based on the use of classical PI controller. Finally, conclusions are in Section 5.

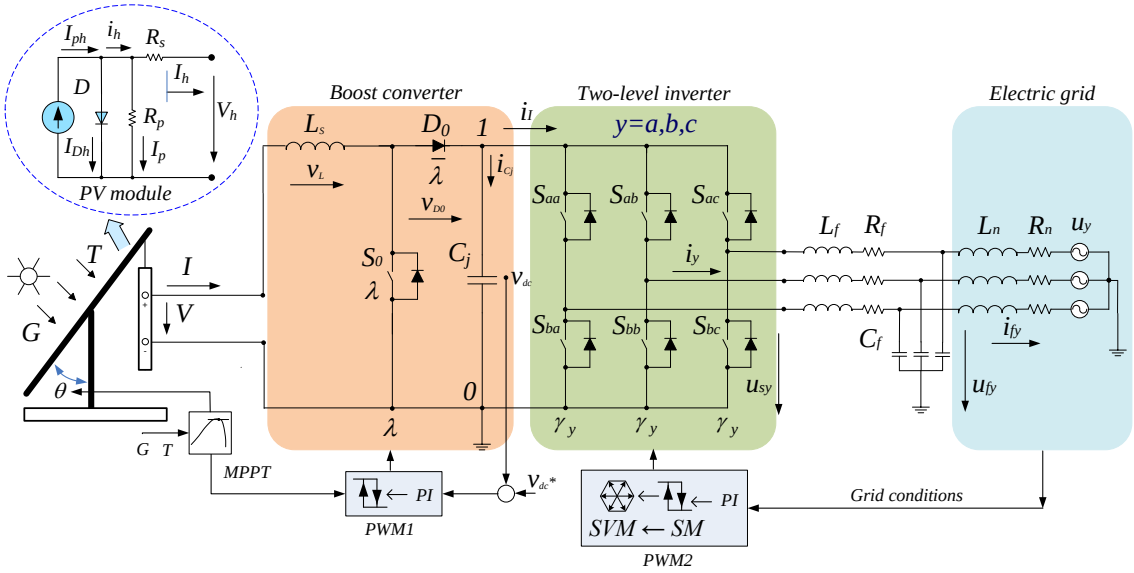

Fig. 1. PV system integrated into the grid by a TwLI.

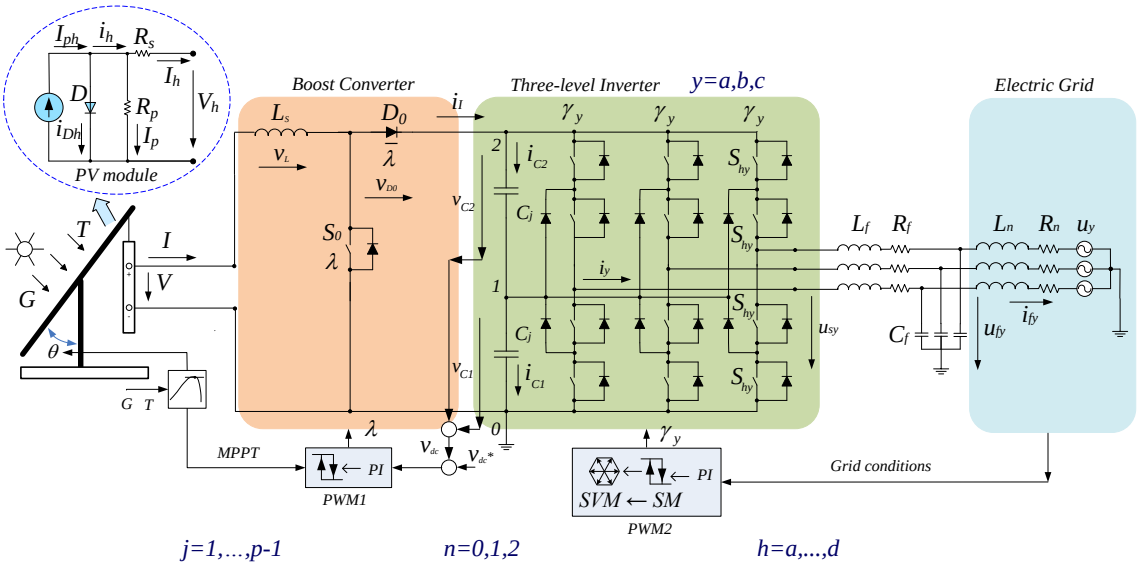

Fig. 2. PV system connected to the grid by ThLI.

2. Modelling

The modelling for the PVsy is a combination of an equivalent electric circuit for the PV module with the models for the boost converter and for the unavoidable interface necessary to inject the PV energy into the EGr. This unavoidability is due to the fact that the EGr is an alternate current one and the PV energy is a source of continuous current. Two configurations for the PVsy are modelled characterized by the PEltr converter used in the interface with the EGr: a TwLI and a ThLI. The configuration for the PVsy integrated into the EGr by a TwLI is shown in Fig. 1. The PVsy linked to the EGr by a ThLI is shown Fig. 2.

2.1. PV Module

The solar cells are considered to be subjected to the same G solar irradiance and T temperature of the semiconductor. Hence, the equivalent circuit of a cell is also the one for any association of cells with a convenient parameters transformation. The PV module equivalent circuit is shown in Fig. 3.

The current i_h is given by:

$$i_h \equiv I_h + (V_h + R_s I_h)/R_p \tag{1}$$

where h is an index linked with operation conditions: $h = oc$, open circuit; $h = sc$, short circuit; and $h = mx$, MPP conditions. The diode D current i_{Dh} [11] is given by:

$$i_{Dh} \equiv I_0\, e_h \tag{2}$$

where I_0 is the diode reverse bias current and e_h is defined [11] by:

$$\ln(e_h + 1) \equiv \gamma (V_h + R_s I_h) \tag{3}$$

where γ is given by $\gamma \equiv 1/mV_T$, m is the ideality factor, V_T is the junction thermal voltage given by the Boltzmann constant K times T divided by the electron charge.

Also, the current i_h is given by:

$$i_h \equiv I_S - i_{Dh} \tag{4}$$

A matrix formulation of (4) combining the conditions at open circuit, short circuit and MPP conditions [11] can be given by:

$$\begin{bmatrix} 1 & -e_{oc} & -1 \\ 1 & -e_{sc} & 0 \\ 1 & -e_{mx} & 0 \end{bmatrix} \begin{bmatrix} I_s \\ I_0 \\ i_{oc} \end{bmatrix} = \begin{bmatrix} 0 \\ i_{sc} \\ i_{mx} \end{bmatrix} \tag{5}$$

The MPP of a PVsy depends on G and T, at the MPP conditions the conversion is attained at the highest efficiency, implying the satisfaction of the relation given by:

$$-\left.\frac{dI}{dV}\right|_{mx} = \frac{I_{mx}}{V_{mx}} \tag{6}$$

Also, at MPP conditions holds the equality [11] given by:

$$\gamma V_{oc} i_{mx}^{sc} (I_{mx} - \delta)(e_{mx} + 1) - \delta\, i_{oc} e_{sc}^{mx} = 0 \tag{7}$$

where δ is defined [11] by:

$$\delta = \frac{\gamma V_{oc} i_{mx}^{sc} (e_{mx} + 1)}{\gamma V_{oc} i_{mx}^{sc} (e_{mx} + 1) + i_{oc} e_{sc}^{mx}} I_{mx} \tag{8}$$

and δ has to satisfy the relation [11] given by:

$$0 < \delta < I_{mx} \tag{9}$$

At open circuit conditions i_{oc} has to satisfy the relation [11] given by:

$$\frac{V_{oc}}{2V_{mx}}(i_{mx} - I_{mx}) < i_{oc} < i_{mx}\frac{V_{oc}}{2V_{mx}} \tag{((10)}$$

The ideality factor m for a cell is assumed to between 2/3 and 2. An ideality factor of 2/3 is due to the Auger recombination: a type of recombination between an electron and a hole in a band-to-band transition giving energy to another electron or hole. While an ideality factor of 2 is due to band to band high level injection or depletion region recombination [11]. Hence, the boundaries for γ [11] are given by:

$$\frac{1}{2V_T} \le \gamma \le \frac{3}{2V_T} \tag{((11)}$$

The five parameters *Rp*, *Rs*, γ, *Iph*, I_0 define the mathematical model for the PV cell equivalent circuit with a single-diode, shunt and series resistances. The General Algebraic Modeling System (GAMS) is used to code a mathematical programming problem for finding these parameters and the free solver COUENNE-Convex Over and Under Envelopes for Nonlinear Estimation for global solution of nonlinear programs is a convenient option due to involvedness on the formulation of the problem. The input data is at STC and is given by the producer of the PV module as technical data.

AnI-V characteristic curve associated with the equivalent circuit of five parameters [11] obeys the relation given by:

$$I = I_{ph} - I_0(e^{\gamma(V + IR_S)} - 1) - (V + IR_S)/R_p \tag{12}$$

Relation (12) cannot be explicit solved in order to the variables, i.e., in order to I or to V. Hence, numeric methods are normal employed to draw I-V characteristics curves. In this paper, (12) is coded in Matlab/Simulink for assessing the I-V characteristic curves using the iterative method of Newton-Raphson.

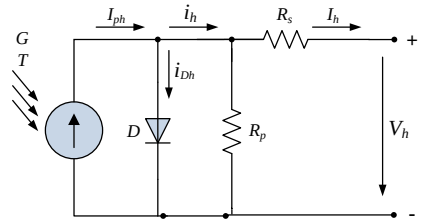

Fig. 3. Equivalent circuit for a PV module

2.2. MPPT Algorithm

The criterion for MPPT is to follow the condition given by $\partial P/\partial V = 0$, i.e., if the condition is met, then the algorithm has found the MPP point. But typically the algorithm iterates around that condition until eventually converges. The iterations procedures are as follow: if $\partial P/\partial V = 0$, no change is made in the out voltage; if $\partial P/\partial V > 0$, an incremental adjustment is set in order to increase the out voltage, i.e., in the direction of the MPP; if $\partial P/\partial V < 0$, an adjustment is set in order to decrease the out voltage to be in the right tracking for the MPP [8]. The Flowchart for the MPPT algorithm used for the PVsy is shown in Fig. 4.

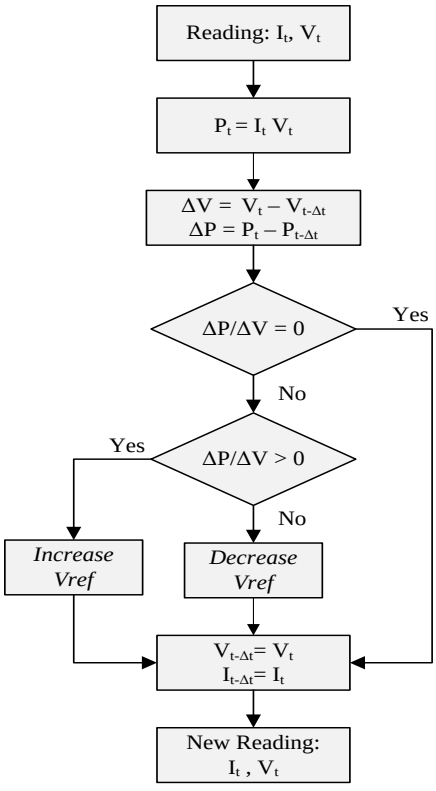

Fig.4. Flowchart for the MPPT algorithm

2.3. DCB Converter

The configuration of the DCB converters is shown in Fig. 1 and Fig. 2. The DCB converter has one unidirectionalcommanded IGBT S_0. The DCB converter is linked between the PV modules and a capacitor bank. This capacitor bank is then connected to a TwLI or a ThLI. The switching of the DCB converter is given by the switching variable (SwV) λ that identifies the state of the IGBT S_0 on the DCB converter and by the SwV $\bar{\lambda}$ used to identify the state of the diode D_0 of the boost. But to emulate the action of the boost converter these variables are not independent [12]. The two conditions to be satisfied by the switching variable of the DCB are given by:

$$\begin{cases} \lambda = 1 \text{ and } \bar{\lambda} = 0 \ (S_0 = 1 \text{ and } D_0 = 0) \\ \lambda = 0 \text{ and } \bar{\lambda} = 1 \ (S_0 = 0 \text{ and } D_0 = 1) \end{cases} \tag{13}$$

The current I is given by:

$$\frac{dI}{dt} = \frac{1}{L_s}[\mathrm{V} - \bar{\lambda}\ (\mathrm{v_{D0}} + v_{dc})\ ] \tag{14}$$

where $\mathrm{v_{D0}}$ is the diode forward voltage at direct current, v_{dc} is the capacitor voltage. The capacitor voltage v_{dc} is given by:

$$\frac{dv_{dc}}{dt} = \frac{1}{C}(\bar{\lambda}\ \mathrm{I} - i_I) \tag{15}$$

where i_I is the current injected into the inverter.

2.4. TwLI

The configuration of the TwLI is shown in Fig. 1. The inverter has $p = 2$ levels. The TwLI links a capacitor bank and a filter (second order filter). The filter is then linked to the EGr. A three-phase active symmetrical circuit models the EGr. This inverter is a DC-AC converter with 6 commanded IGBT's S_{hy}. The two IGBT's that are connected to the same phase represent a converter leg y. The switching function of a IGBT is given by the SwV γ_y, representing the IGBT h state in the leg y. The IGBT is identified by an index h, where $h \in \{a,b\}$. The inverter leg is identified by an index y, where $y \in \{a,b,c\}$. Each leg y of the converter is associated with a variable [13] n_y given by:

$$n_y = \begin{cases} 1, \ (S_{ay} = 1 \text{ and } S_{by} = 0) \\ 0, \ (S_{ay} = 0 \text{ and } S_{by} = 1) \end{cases} \quad y \in \{a, b, c\} \tag{16}$$

A restriction is imposed for each leg y [13]. The restriction is given by:

$$\sum_{i=1}^{2} S_{hy} = 1 \quad h \in \{a,b\} \ y \in \{a, b, c\} \tag{17}$$

The current injected at the inverter i_I is given by:

$$i_I = \sum_{y=a}^{c} n_y i_y \quad n \in \{1, 0\} \;\; y \in \{a, b, c\} \tag{18}$$

The inverter output voltage u_{sy} is given by:

$$u_{sy} = \frac{1}{3}(2n_y - \sum_{\substack{j=a \\ j \neq y}}^{c} n_j)\, v_{dc} \quad n \in \{0, 1\} \;\; y \in \{a, b, c\} \tag{19}$$

The state equation of the voltage v_{dc} is given by:

$$\frac{dv_{dc}}{dt} = \sum_{j=1}^{p-1} \frac{1}{C_j} i_{cj} \quad j \in \{1, ..., p-1\} \;\; n \in \{0, 1\} \tag{20}$$

More detailed information about this modelling is in [13].

2.5. ThLI

The ThLI configuration is shown in Fig. 2. This inverter has $p = 3$ levels. The inverter is a DC-AC converter with 12 IGBT's S_{hy}. The four IGBT's that are connected to the same phase represent a converter leg y. The switching voltage level variable n_y, where $0 \leq n_y \leq (p-1)$, identifies the IGBT h state, with $h \in \{a, b, c, d\}$. The index y with $y \in \{a, b, c\}$ identifies a leg. For the SwV of the voltage level on the leg $y \in \{a, b, c\}$ at each level [14] there are three valid conditions given by:

$$n_y = \begin{cases} 2, & (S_{ay} \text{ and } S_{by}) = 1 \quad \text{and} \quad (S_{cy} \text{ or } S_{dy}) = 0 \\ 1, & (S_{by} \text{ and } S_{cy}) = 1 \quad \text{and} \quad (S_{ay} \text{ or } S_{dy}) = 0 \\ 0, & (S_{cy} \text{ and } S_{dy}) = 1 \quad \text{and} \quad (S_{ay} \text{ or } S_{by}) = 0 \end{cases} \tag{21}$$

The switching voltage level variable n_y is also used to identify the vector (level-1) in the calculation of the converter output voltage u_{sy}. The inverter output voltage u_{sy} in function of v_{dc} [14] is given by:

$$u_{sy} = \frac{1}{6}(2n_y - \sum_{\substack{j=a \\ j \neq y}}^{c} n_j)\, v_{dc} \quad n \in \{0, 1, 2\} \;\; y \in \{a, b, c\} \tag{22}$$

For each capacity bank the current i_{cj} [14] is given by:

$$i_{cj} = i_I - \sum_{y=a}^{c} \delta_{ny} i_y \quad j \in \{1, \ldots, p-1\} \;\; y \in \{a, b, c\} \tag{23}$$

where the auxiliary variable δ_{ny} [14] is given by:

$$\delta_{ny} = \begin{cases} 0 & j > n_y \\ 1 & j \leq n_y \end{cases} \quad j \in \{1, \ldots, p-1\} \;\; n \in \{0, 1, 2\} \tag{24}$$

The state equation of the voltage v_{dc} [14] is given by:

$$\frac{dv_{dc}}{dt} = \sum_{j=1}^{p-1} \frac{1}{C_j} i_{cj} \quad j \in \{1, \ldots, p-1\} \tag{25}$$

More detailed information about this modelling is in [14].

2.6. Electric Grid

The EGr is modelled by a triphasic active symmetrical independent voltage source linked to an inductor and resistance emulating the short circuit impedance of the EGr. This model is shown in Fig. 1 and Fig. 2. The EGr injected phase current i_{fk} is given by:

$$\frac{di_{fy}}{dt} = \frac{1}{L_n}(u_{fy} - R_n i_{fy} - u_y) \quad y \in \{a, b, c\} \tag{26}$$

Where u_{fy} is the value for the independent voltage source, R_n and L_n are respectively the resistive part and the inductive part of the short-circuit impedance where the PV array is connected.

3. Control Strategy

PI controllers implement the controller strategy considered in the simulation for the operation of the PVsy with two-level or three-level inverter in order to follow the references. Power converters (PwCo) are mutable structures due to the transistors on/off states and the PWMo by SVMo associated with SMCo is used to control the converter. The SMCo strategy is an option known by the advantage of having smart features, e.g., considerable robustness to parametric unreliability due to partial shading or EGr disturbances [11,13,14]. The aim of the SMCo is to change the system structure allowing the system to slide along a defined sliding surface. The control strategy of the PVsy with DCB and two-level or three-level power converter topologies using classical PI controllers has the diagram in box PWM1 and in box PWM2 shown in Fig. 1 or in Fig. 2. The convenient vector selection to ensure the converters stability, after the hysteresis comparator processing in the blocks of the SMCo and SVMo are given in [11,13,14]. The output space vectors in the $\alpha\beta$ plane for level *0* and level *1* for the TwLI [12,13] are shown in Fig. 5.The output space vectors for level *0*, level *1* and level *2* for the ThLI [13,14] are shown in Fig. 6.

The SMCo is of particular interest in switching power inverters, with their variable structure, guaranteeing the

correct choice of the space vectors. Changing the system structure allows the system sliding along a defined sliding surface $A(e_{\alpha\beta},t)$. There are current IGBT's physical restrictions, i.e., they cannot operate at infinite frequency. Likewise, a switching frequency with a finite value will have an error between his control value and the reference value $e_{\alpha\beta}$. The system sliding along the surface $A(e_{\alpha\beta},t)$ is guaranteed if the trajectory satisfied the following condition [13,14] given by:

$$A(e_{\alpha\beta},t)\frac{dA(e_{\alpha\beta},t)}{dt}<0 \tag{27}$$

The selection to ensure stability on the TwLI [13] is shown in Table 1.

Table 1. Output vectors selection for the TwLI

$\delta_\beta \setminus \delta_\alpha$	-1	0	1
-1	e_1	$e_1;f_1$	f_1
0	g_1	$a_0;h_0$	b_1
1	c_1	$c_1;d_1$	d_1

The selection to guarantee stability on the ThLI [14] is shown in Table 2.

Table 2. Output vectors selection for the ThLI

$\delta_\beta \setminus \delta_\alpha$	-2	-1	0	1	2
-2	p_2	p_2	w_2	o_2	o_2
-1	f_1	$f_1;d_1;k_1$	$d_1;k_1;m1;y2$	$m_1;y_2;u_2$	u_2
0	$\tilde{n}_2$	$b_1;g_1$	$a_0;h_0;z_0$	$i_1;n_1$	s_2
1	x_2	$c_1;x_2;t_2$	$c_1;e_1;l_1;t_2$	$e_1;l_1;j_1$	j_1
2	r_2	r_2	v_2	q_2	q_2

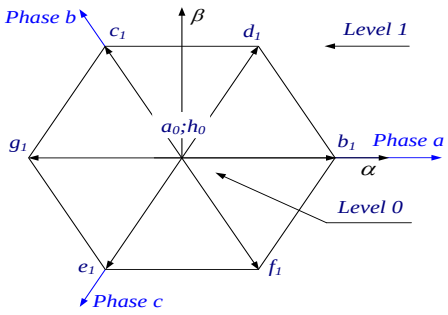

Fig. 5. TwLI, output space vectors.

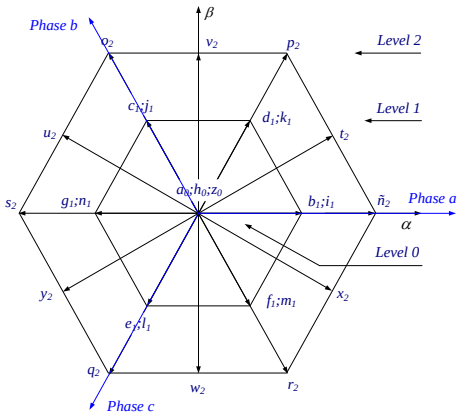

Fig. 6. ThLI, output space vectors.

4. Case study

The models for the PVsy using the five parameters cell equivalent circuit, the DCB, respectively the TwLI or the ThLI topologies shown in Fig. 1 or Fig. 2, the MPPT algorithm, and the control strategy are programmed in Matlab/Simulink to carried out the simulations for the case study. The measure of the voltage and the current harmonic content at the inverter output is carried out with the experimental system by appropriated instrumentation and for the results obtained by the simulation with the discrete Fourier transform (DFT). The DTF is given by:

$$Y(k)=\sum_{n=0}^{N-1}e^{-j2\pi\, k\, n/N}\; y(n) \quad \text{for} \quad k=0,\ldots,N-1 \tag{28}$$

where $y(n)$ is the output signal, $Y(k)$ is a complex number representing the phase and amplitude of the several sinusoidal components of $y(n)$. Also, the total harmonic distortion (THD) is given by:

$$\text{THD}\,(\%)=100\,\frac{\sqrt{\sum_{H=2}^{50}Y_H^2}}{Y_F} \tag{29}$$

where Y_F is the root mean square (RMS) value of the fundamental component and Y_H is the RMS value for the harmonic H. The simulation is carried out for a silicon amorphous PV module situated in LNEG, with the coordinates 38°46'18.50' N, 9°10'38.50' W. The STC data for the amorphous silicon PV module Kaneka KA 58 [15] is shown in Table 3.

Table 3. Data for Kaneka KA58 solar module at STC

Technology	V_{MP}^*	I_{MP}^*	V_{oc}^*	I_{sc}^*
Amorphous	63 V	0.92 A	85 V	1.12 A

The switching frequency for IGBTs is 5 kHz. The experimental system is located in LNEG, Lisbon, Portugal. The PVsy's are connected via the electrical switchboard to the EGr of 230/400 V at 50 Hz EGr by the commercial inverter based on the use of classical PI controller, with a nominal AC power of 3.3 kW. The experimental PVsy's description and configurations are shown in Table 4.

Table 4. Experimental PV systems

Parameter	PV system
Module capacity	60 Wp
Manufacturer/model	Kaneka GEA 60
Technology	a-Si
Installed capacity	3.0 kWp
String configuration	5 modules×10 strings
Inverter	SolarStocc PS4000HV
Inverter Rated capacity	3.3 kW

The irradiation and ambient temperature test data for the experimental systems is shown in Table 5.

Table 5. Irradiance and ambient temperature

Irradiance	800 W/m^2
Ambient temperature	13 ºC
Date, hour	08/02/2012, 12:11

The simulation results are compared with experimental observation carried out using the amorphous PV technology. The simulated, green, and experimental, blue, curves for I-V; the absolute error, red, and MPP at STC conditions are shown in Fig. 7.The simulated, green, and experimental, blue, curves for P-V; the absolute error, red, and MPP at STC conditions are shown in Fig. 8.

Both Fig. 7 and Fig. 8 favour the agreement of the identified parameters for the equivalent circuit with the performance data of the real PV module. Particularly, in the region of normal operation, i.e., the neighborhood of the MPP, the mean square error is about 0.45 W^2 for the range of voltage [60 V, 70 V] in the neighborhood of the MPP voltage. So, the agreement is convenient for practical purposes [16].. The current injected into the EGr, simulated, green, experimental, blue, and the absolute error on the current are shown in Fig. 9.

The simulations root mean square error (RMSE) for the I-V characteristic curve, P-V curve and current injection for the EGr -connected system is shown in Table 6.Both RMSE are a small relative value of the respective rated values, showing that the modelling is appropriated for describing the PVsy connected to the EGr by the commercial inverter. For the EGr -connected system, the harmonic behaviour for the current injection, experimental data in blue and simulated with two-level or three-level inverters in green, are shown in Fig. 10 and Fig. 11.

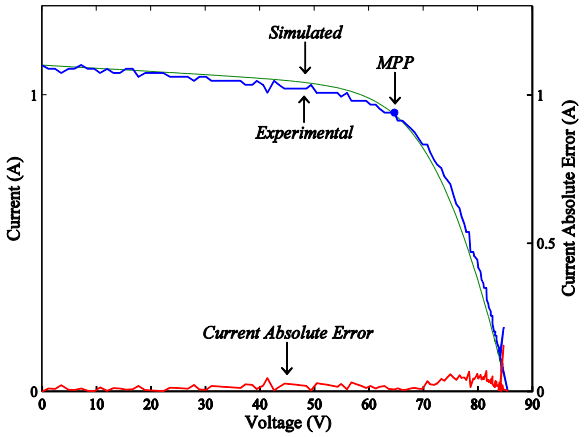

Fig. 7. I-V curves simulated and experimental.

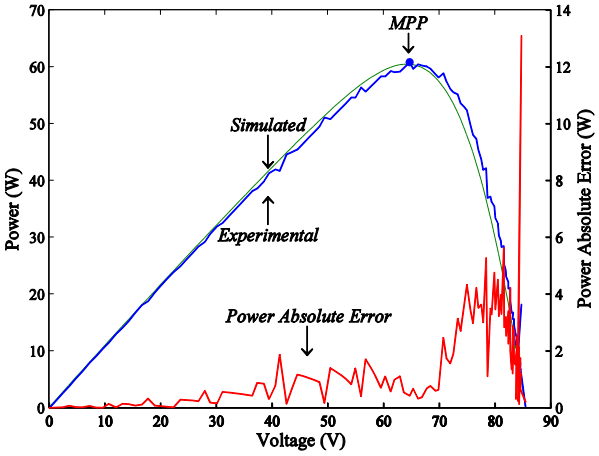

Fig. 8. P-V curves simulated and experimental.

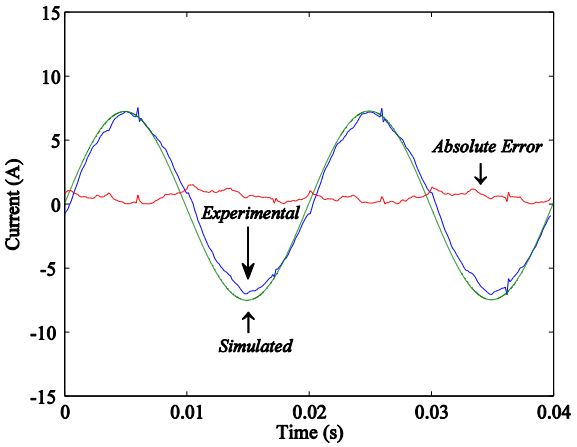

Fig. 9. Electric grid current injected.

Table 6. Simulations root mean square error (RMSE)

Simulation	I-V Curve	P-V Curve	Current injected into the grid
RMSE	0.0293 A	2.2328	0.6656 A

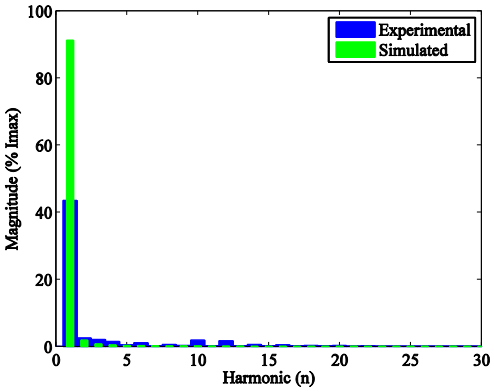

Fig. 10..DFT of the current injection experimental and simulated with TwLI

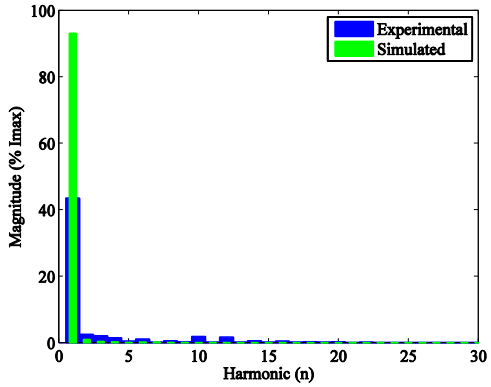

(b)

Figure 11. DFT of the current injection experimental and simulated with ThLI.

Figures 10 and 11 allow concluding that: the PVsy with ThLI performs better than the one with the TwLI; the percentage of the fundamental harmonic calculated by the DFT for the simulated current injection has very favourable results, about 93%. The comparison between the harmonic percentage of the fundamental component for the current injection for the experimental and the simulated results with TwLI or ThLI are shown in Table 7.

Table 7. Experimental and simulated current harmonics

Harmonic(n)	Experimental (%)	Two-level (%)	Three-level (%)
1	79.5	91.2	93.1
2	0.2	1.5	1.0
3	0.7	0.7	0.4
4	0.1	0.4	0.25
5	0.5	0.2	0.1
6	0.1	0.3	0.2
7	0.6	0.2	0.2
8	0.1	0.1	0.1
9	0.3	0.2	0.1
10	0.1	0.1	0.1
11	0.3	0.2	0.1

The fundamental component percentage calculated with DFT for the simulated current injection into the EGr with ThLI is 93.1%, with TwLI is 91.2% and for the experimental current injection data is 79.5%. Those differences between the respective percentages are believed to happen impart due to the fact that the EGr is not a perfect ideal source of voltage. Additionally, the observation of Table 7 is in favour that the current injection for the PVsy with TwLI or ThLI based in classical PI control presents a content of high order harmonics relatively low due to the second order filter.The comparison between the THD for the current experimental and the simulated results with two-level or three-level inverters are shown in Table 8.

Table 8. Experimental and simulated current harmonics

Experimental (%)	Two-level (%)	Three-level (%)
4.17	5.005	2.41

The current injection THD is about 2.4 % for the PVsy with ThLI. Hence, the system has an adequate performance in what regards the fact that the current output THD is lower than the 5% limit required by the IEEE-519 standard.

5. Conclusions

Simulation studies on PV systems are essential to assists the engineers in what regards extracting the maximum energy, anticipating performance and deciding convenient measures to avoid malfunctions. A PV system modelling with DCB and TwLI or ThLI topology is proposed using the equivalent five parameter for PV modules; and DCB with two-level or three-level power inverter topology modelling, assuming a control strategy by PI controllers and PWMo by SVMo associated with SMCo. The PV system with ThLI presents a better behaviour in comparison with the system with TwLI. The data comparison between simulation of a PV system integrated models and experimental results during the in situ operation is in favour of this contribution as an integrated relevant modelling.

The application of this modelling to a case study on a amorphous silicon solar module Kaneka KA 58 with a commercial inverter and a convenient filtering allows to anticipate a THD for the output current lower than the 5% limit required by the IEEE-519 standard, for the PV system with DCB and two-level or three-level power inverter topologies. Although disregarding in the simulations the fact that the EGr is not a perfect source of energy, the experimental results show a tolerable concordance with the simulated ones.

Acknowledgements

This work is funded by Portuguese Funds through the Foundation for Science and Technology-FCT under the project LAETA 2015-2020, reference UID/EMS/50022/2013.

References

[1] A. Poullikas, "A comparative assessment of net metering and feed in tariff schemes for residential PV systems", *Sust. Energy Technologies and Assessments*, vol. 3, pp. 1–8, 2013.

[2] J. Peças Lopes, N. Hatziargyriou, J. Mutale, P. Djapic, and N. Jenkins, "Integrating distributed generation into electric power systems: a review of drivers, challenges and opportunities", *Electric Power Systems Research*, vol. 77, pp. 1189–1203, 2007.

[3] F. Blaabjerg, Z. Chen, and S.B. Kjaer, "Power electronics as efficient interface in dispersed power generation systems", *IEEE Transactions Industrial Electronics*, vol. 19, pp. 1184–1194, 2007.

[4] F. Blaabjerg, R. Teodoresco, M. Liserre, and A.V. Timbus, "Overview of control and grid synchronization for distributed power generation systems", *IEEE Transactions Industrial Electronics*, vol. 53, pp. 1398–1409, 2006.

[5] T. Salmi, M. Bouzguenda, A. Gastli, and A. Masmoudi, "MATLAB/Simulink based modelling of solar photovoltaic cell", *International Journal of Renewable Energy Research*, vol. 2, pp. 213–218, 2012.

[6] H.A. Kazem, and T. Khatib, "Techno–economical assessment of grid connected photovoltaic power systems productivity in Sohar, Oman", *Sust. Energy Tech. and Assessments*, vol. 3, pp. 61–65, 2013.

[7] V. FernãoPires, J.F. Martins, D. Foito, and C. Hão, "A grid connected photovoltaic system with a multilevel inverter and a Le-Blanc transformer", *International Journal of Renewable Energy Research*, vol. 2, pp. 84–91, 2012.

[8] R.J. Pereira, R. Melício, V.M.F. Mendes, and A. Joyce", Effect of shading on series solar modules: simulation and experimental results", *Procedia Technology*, vol. 17, pp. 295–302, 2014.

[9] E. Koutroulis, and F. Blaabjerg, "Methods for the optimal design of grid-connected PV inverters", *International Journal Renewable Energy Research*, vol. 1, pp. 54–64, 2011.

[10] Y. Yang, and F.P. Zhao, "Adaptive perturb and observe MPPT technique for grid-connected photovoltaic inverters", *Procedia Engineering*, vol. 23, pp. 468–473, 2011.

[11] L. Fialho, R. Melício, V.M.F. Mendes, S. Viana, C. Rodrigues, A. Estanqueiro, "A simulation of integrated photovoltaic conversion into electric grid", *Solar Energy*, vol. 110, pp. 578–594, 2014.

[12] L. Fialho, R. Melício, V.M.F. Mendes, L. Rodrigues, S. Viana, and A. Estanqueiro, "Simulation of a-Si PV System Linked to the Grid by DC-DC Boost and Two-level Converter", *16th International Power Electronics and Motion Control Conference and Exposition – PEMC 2014*, Antalya, Turkey, pp. 21–24, September 2014.

[13] R. Melício, and V.M.F. Mendes, "Simulation of power converters for wind energy systems", *InformaciónTecnológica*, vol. 18, pp. 25–34, July–August 2007.

[14] M. Seixas, R. Melício, and V.M.F. Mendes, "Fifth harmonic and sag impact on PMSG wind turbines with a balancing new strategy for capacitor voltages", *Energy Conversion and Management*, vol. 79, pp. 721–730, March 2014.

[15] Kaneka Photovoltaic Products Inform.http://www.pv.kaneka.co.jp.

[16] D.P. Hohm, and M.E. Ropp, "Comparative study of maximum power point tracking algorithms", *Progress in Photovoltaics: Research and Applications*, vol. 11, pp. 47-62, January 2003.